AGU PUBLICATIONS

JGR

Journal of Geophysical Research: Space Physics

RESEARCH ARTICLE

10.1002/2013JA019421

Key Points:
- Compare simulations of 2009 SSW in four whole atmosphere models
- The simulations reveal different dynamics at MLT altitudes
- Differences are attributed primarily to gravity wave drag parametrizations

Correspondence to:
N. M. Pedatella,
nickp@ucar.edu

Citation:
Pedatella, N. M., et al. (2014), The neutral dynamics during the 2009 sudden stratosphere warming simulated by different whole atmosphere models, *J. Geophys. Res. Space Physics*, *119*, 1306–1324, doi:10.1002/2013JA019421.

Received 6 SEP 2013
Accepted 22 JAN 2014
Accepted article online 28 JAN 2014
Published online 18 FEB 2014

The neutral dynamics during the 2009 sudden stratosphere warming simulated by different whole atmosphere models

N. M. Pedatella[1], T. Fuller-Rowell[2], H. Wang[2], H. Jin[3], Y. Miyoshi[4], H. Fujiwara[5], H. Shinagawa[3], H.-L. Liu[1], F. Sassi[6], H. Schmidt[7], V. Matthias[8], and L. Goncharenko[9]

[1]High Altitude Observatory, National Center for Atmospheric Research, Boulder, Colorado, USA, [2]CIRES, University of Colorado Boulder, Boulder, Colorado, USA, [3]National Institute of Information and Communications Technology, Tokyo, Japan, [4]Department of Earth and Planetary Sciences, Kyushu University, Fukuoka, Japan, [5]Faculty of Science and Technology, Seikei University, Tokyo, Japan [6]Space Science Division, Naval Research Laboratory, Washington DC, USA, [7]Max Planck Institute for Meteorology, Hamburg, Germany, [8]Leibniz Institute for Atmospheric Physics at Rostock University, Kühlungsborn, Germany, [9]Haystack Observatory, Massachusetts Institute of Technology, Westford, Massachusetts, USA

Abstract The present study compares simulations of the 2009 sudden stratospheric warming (SSW) from four different whole atmosphere models. The models included in the comparison are the Ground-to-topside model of Atmosphere and Ionosphere for Aeronomy, Hamburg Model of the Neutral and Ionized Atmosphere, Whole Atmosphere Model, and Whole Atmosphere Community Climate Model Extended version (WACCM-X). The comparison focuses on the zonal mean, planetary wave, and tidal variability in the middle and upper atmosphere during the 2009 SSW. The model simulations are constrained in the lower atmosphere, and the simulated zonal mean and planetary wave variability is thus similar up to ~1 hPa (50 km). With the exception of WACCM-X, which is constrained up to 0.002 hPa (92 km), the models are unconstrained at higher altitudes leading to considerable divergence among the model simulations in the mesosphere and thermosphere. We attribute the differences at higher altitudes to be primarily due to different gravity wave drag parameterizations. In the mesosphere and lower thermosphere, we find both similarities and differences among the model simulated migrating and nonmigrating tides. The migrating diurnal tide (*DW*1) is similar in all of the model simulations. The model simulations reveal similar temporal evolution of the amplitude and phase of the migrating semidiurnal tide (*SW*2); however, the absolute *SW*2 amplitudes are significantly different. Through comparison of the zonal mean, planetary wave, and tidal variability during the 2009 SSW, the results of the present study provide insight into aspects of the middle and upper atmosphere variability that are considered to be robust features, as well as aspects that should be considered with significant uncertainty.

1. Introduction

Sudden stratospheric warmings (SSWs) are large-scale meteorological disturbances that dramatically impact the dynamics of the high latitude wintertime stratosphere. Interaction of upward propagating planetary waves and the zonal mean flow is the primary generation mechanism for SSWs [*Matsuno*, 1971]. In the stratosphere, SSWs are associated with a rapid increase in the polar temperature, deceleration and occasional reversal of the high latitude eastward winds, and a significant disruption of the polar vortex [*Scherhag*, 1952; *Schoeberl*, 1978; *Limpasuvan et al.*, 2004; *Charlton and Polvani*, 2007]. SSWs are classified as major warmings if the zonal mean zonal wind at 60°N and 10 hPa reverses from eastward to westward. SSWs that only exhibit a deceleration, and not a complete reversal, of the zonal mean zonal winds are considered minor warmings. Major SSWs typically occur in the Northern Hemisphere with a frequency of approximately six events per decade [*Charlton and Polvani*, 2007]. SSW associated disturbances are thus a fairly common feature of the high latitude Northern Hemisphere stratosphere. Although less common, major SSWs can also occur at high latitudes in the Southern Hemisphere during Southern Hemisphere winter [e.g., *Charlton et al.*, 2005].

In addition to influencing the high latitude stratosphere dynamics, SSWs also impact the mesosphere and thermosphere. Accompanying the increase in polar stratospheric temperatures is a significant cooling of the high latitude mesosphere [*Quiroz*, 1969; *Liu and Roble*, 2002; *Cho et al.*, 2004]. Changes in the equatorial and Southern Hemisphere mesosphere are also connected to the high latitude Northern Hemisphere stratosphere [*Karlsson et al.*, 2009; *Tan et al.*, 2012], and SSWs can therefore influence the mesosphere globally.

Evidence also exists for lower thermosphere warming during SSWs [*Liu and Roble*, 2002; *Goncharenko and Zhang*, 2008; *Funke et al.*, 2010]. Though the impact of SSWs on the mesosphere and lower thermosphere (MLT) is well understood, it remains unclear what, if any, effect SSWs have on the upper thermosphere. *Liu et al.* [2011, 2013] present results indicating a cooling of the thermosphere during the 2009 SSW; however, this result was attributed to the influence of varying geomagnetic activity by *Fuller-Rowell et al.* [2011a]. Additional studies are therefore necessary in order to develop a clear understanding of the potential impact of SSWs on the upper thermosphere.

Studies of the impact of SSWs on the upper atmosphere have recently been extended to the ionosphere, where SSW-related disturbances have been found in ion temperatures [*Goncharenko and Zhang*, 2008], vertical plasma drift velocities [*Chau et al.*, 2009, 2010; *Fejer et al.*, 2010], electron densities [*Lin et al.*, 2012], and total electron content (TEC) [*Goncharenko et al.*, 2010a, 2010b]. Modulation of atmospheric tides is the generally accepted mechanism for generating the ionospheric perturbations during SSWs [*Chau et al.*, 2012]. However, the specific tidal changes, and their impact on the ionosphere, are not yet fully understood. Among the proposed mechanisms are changes in solar migrating tides [*Fuller-Rowell et al.*, 2011b; *Jin et al.*, 2012; *Lin et al.*, 2012], nonmigrating tides [*Pedatella and Forbes*, 2010], and the lunar semidiurnal tide [*Fejer et al.*, 2010]. A number of studies have also focused on how SSWs may introduce variability in these tides. Changes in the solar semidiurnal migrating tide (*SW*2) are thought to be due to SSW induced changes in the distribution of ozone which influences the generation of the *SW*2 [*Goncharenko et al.*, 2012], changes in tidal propagation due to changes in the zonal mean atmosphere [*Jin et al.*, 2012], and/or interaction with planetary waves [*Liu et al.*, 2010a]. The enhancement in certain nonmigrating tides is attributed to increased planetary wave activity during SSWs, which facilitates the generation of nonmigrating tides through nonlinear planetary wave-tide interactions [*Liu et al.*, 2010a]. Changes in the zonal mean atmosphere are thought to lead to enhancements in the lunar semidiurnal tide [*Forbes and Zhang*, 2012]. The actual changes are complex, and the ionosphere perturbations during SSWs may be driven by a combination of the aforementioned mechanisms [*Pedatella and Liu*, 2013].

Numerical models have proven to be an essential tool for studying the middle and upper atmosphere response to SSWs. This is primarily due to the fact that, owing to a lack of observations, numerical models are the only tool for studying the short-term (i.e., days to weeks) variability that occurs in the migrating and nonmigrating tides. Though ground-based radar observations have provided insight into the MLT tidal variability during SSWs [*Matthias et al.*, 2012; *Sridharan et al.*, 2012], ground-based observations at a single location are unable to distinguish between migrating and nonmigrating tides and do not provide the necessary global view of the tidal variability. Satellite observations can provide global coverage; however, current satellite observations lack the necessary temporal resolution to study day-to-day tidal variability. Numerical models are thus the primary source for gaining insight into the dynamical variability of the middle and upper atmosphere during SSWs. The recent development of whole atmosphere models [*Akmaev*, 2011] has significantly aided the study of middle and upper atmosphere variability during SSWs. Whole atmosphere models extend from the surface into the thermosphere and are thus well suited for studying the global response of the lower, middle, and upper atmosphere to SSWs. Whole atmosphere models also provide the opportunity to potentially predict upper atmosphere variability due to SSWs several days in advance. This is particularly important for the ionosphere where the several day forecast skill is extremely low [e.g., *Schunk et al.*, 2012]. Using "free-running" versions of whole atmosphere models, several recent studies have elucidated the average effects of SSWs on the MLT [*Fuller-Rowell et al.*, 2010; *Miller et al.*, 2013; *Pedatella et al.*, 2012]. Simulations by *Zülicke and Becker* [2013] that resolved large parts of the gravity wave spectrum demonstrated that changes in mesospheric winds and temperatures are driven by gravity wave drag. By adequately constraining the lower atmosphere portion of the model, whole atmosphere models have also provided insight into the dynamical variability during real SSW events [e.g., *Jin et al.*, 2012; *Wang et al.*, 2011; *Sassi et al.*, 2013; *McLandress et al.*, 2013].

Although real SSW events have been simulated in different whole atmosphere models, validating the results at higher altitudes (i.e., in the mesosphere and thermosphere) remains difficult. This is especially the case for day-to-day variability in migrating and nonmigrating tides owing to the lack of available observations to compare with the model simulations. Furthermore, the lack of comprehensive observations of the dynamical fields in the middle and upper atmosphere inhibits fully constraining the atmospheric state at these altitudes through data assimilation, leading to simulation results at these altitudes that are potentially highly influenced by specific model parameterizations. There thus remains significant uncertainty in the simulation

results, and this can potentially lead to conflicting results on how SSWs affect the middle and upper atmosphere [e.g., *Liu et al.*, 2011; *Fuller-Rowell et al.*, 2011a]. To gain a better understanding of the current state of modeling the middle and upper atmosphere response to SSWs in whole atmosphere models, the present study directly compares results from four different whole atmosphere models. The comparison focuses on the major SSW that occurred during late January and early February 2009. The 2009 SSW was the strongest and longest lasting SSW to occur in the modern era [e.g., *Manney et al.*, 2009], and it is thus well suited for studying the coupling between SSWs and variability in the middle and upper atmosphere. We compare simulations from the Ground-to-topside model of Atmosphere and Ionosphere for Aeronomy (GAIA), Hamburg Model of the Neutral and Ionized Atmosphere (HAMMONIA), Whole Atmosphere Model (WAM), and Whole Atmosphere Community Climate Model Extended version (WACCM-X). Through illustration of the similarities, and differences, among the models we are able to develop an understanding of the common features of the middle and upper atmosphere response to SSWs, as well as aspects of the response that may be highly uncertain. Furthermore, the present study seeks to understand what mechanisms may be responsible for driving the differences among the models with an aim toward improving future model simulations.

The remainder of the paper is organized as follows. Section 2 provides a brief description of the different models and how they are constrained to simulate the 2009 SSW. The simulated zonal mean variability is presented in section 3.1 and is compared with Aura Microwave Limb Sounder (MLS) temperature observations. Results for planetary waves are discussed in section 3.2. Section 3.3 presents results for selected tidal components. Our overall conclusions are summarized in section 4.

2. Model Simulations

The present study compares model results from GAIA, HAMMONIA, WAM, and WACCM-X. A brief description of each model is provided in the following sections. This is not intended to be a comprehensive description of the individual models, and we focus our attention on aspects that are deemed to be particularly relevant for simulating the middle and upper atmosphere during the 2009 SSW. For detailed descriptions, the reader is referred to the appropriate references. Hourly model output is used in the present study. The results presented in section 3 are obtained based on processing the hourly simulation results with an identical procedure, and there is thus no potential uncertainty due to different analysis methods.

2.1. GAIA

GAIA is a coupled atmosphere-ionosphere model extending from the ground to the exobase ($\sim 1\times10^{-10}$ hPa). GAIA includes neutral atmosphere, ionosphere, and electrodynamics components. Among the models considered in the present comparison, it is thus unique in that it includes a fully coupled ionosphere with electrodynamics. Specific details regarding GAIA, as well as an overview of the 2009 SSW simulations, can be found in *Jin et al.* [2012, and references therein]. GAIA employs a nudging technique to simulate the dynamics of the 2009 SSW. The model is nudged toward meteorological reanalysis fields (surface temperature and pressure, temperature, zonal and meridional winds, and water vapor) from the Japanese 25 year Reanalysis (JRA-25) from the surface to 12 hPa. The model is unconstrained above 12 hPa. The ozone distribution in GAIA is prescribed based on the monthly mean climatology, and thus, any ozone variations during the SSW are not captured in GAIA. The gravity wave parameterizations of *McFarlane* [1987] and *Lindzen* [1981] are used for orographic and nonorographic gravity waves, respectively.

2.2. HAMMONIA

HAMMONIA is an atmospheric general circulation model covering an altitude range from the surface up to 1.7×10^{-7} hPa ($\sim$250 km). *Schmidt et al.* [2006] provide a thorough overview of the chemical, dynamical, and physical processes and parameterizations that are included in HAMMONIA. Note that the present version of HAMMONIA uses 119 vertical layers, in contrast to previous versions that used 67 vertical layers. To simulate the 2009 SSW, HAMMONIA is nudged to the European Center for Medium range Weather Forecasting (ECMWF) temperature, divergence, and vorticity from 850 to 1 hPa, and it is unconstrained above this altitude. Surface pressures from the ECMWF reanalysis are also imposed on the HAMMONIA simulations. HAMMONIA includes a comprehensive chemistry package, and it is thus able to simulate ozone changes that occur during the 2009 SSW. Gravity wave parameterizations of *Hines* [1997a, 1997b] and *Lott and Miller* [1997] are used for the nonorographic and orographic gravity waves, respectively. A comprehensive ionosphere is not included in HAMMONIA. It does, however, include the effects of ion drag through the parameterization of *Hong and Lindzen* [1976].

2.3. WAM

WAM extends the United States National Weather Service Global Forecast System to the upper thermosphere (~1.5×10^{-9} hPa) [*Akmaev et al.*, 2008; *Fuller-Rowell et al.*, 2008]. To constrain the lower atmosphere, a three-dimensional variational (3DVAR) technique is used to perform data assimilation in WAM [*Wang et al.*, 2011]. Note that only lower atmosphere observations are assimilated in WAM, and the observations do not directly impact the simulations above ~0.1 hPa. Similar to the other models, the middle and upper atmosphere in WAM are thus not directly constrained by the data assimilation. Variability in middle atmosphere ozone is included in the WAM simulations. WAM implements gravity wave drag as described by *Alpert et al.* [1988], and vertical variations in the momentum flux occur when the local Richardson number is less than 0.25, or when wave breaking occurs, in which case the momentum flux is reduced according to the *Lindzen* [1981] wave saturation hypothesis. Though it has been used to reproduce the ionosphere response to SSWs using one-way coupling [*Fuller-Rowell et al.*, 2011b], WAM itself does not include an ionosphere, and an empirical ionosphere model is used to specify the ion drag force.

2.4. WACCM-X

WACCM-X covers the altitude range from the surface to the upper thermosphere (2.5×10^{-9} hPa), and a detailed description of WACCM-X can be found in *Liu et al.* [2010b]. An overview of the 2009 SSW WACCM-X simulation used in the present study is provided by *Sassi et al.* [2013]. To simulate the 2009 SSW, WACCM-X is constrained through nudging the dynamical fields toward a merged reanalysis of the Navy Operational Global Atmospheric Prediction System–Advanced Level Physics High Altitude (NOGAPS-ALPHA) and the NASA Modern Era Retrospective Analysis for Research and Applications (MERRA). The nudging is performed from the surface to 0.002 hPa (~ 92 km), and WACCM-X is thus the only model that is directly constrained in the mesosphere. WACCM-X includes an interactive chemistry package, and the ozone variability is thus included in the WACCM-X simulations. The gravity wave drag parameterizations of *McFarlane* [1987] and *Lindzen* [1981] are used for the orographic and nonorographic gravity waves in WACCM-X. Only a simplified ionosphere, including the production and loss of electrons and ions, is included in WACCM-X.

3. Results

3.1. Zonal Mean Variability

Figure 1 shows the daily zonal mean temperature averaged between 70° and 80°N for the model simulations and Aura MLS observations [*Schwartz et al.*, 2008]. Note that in Figure 1, and throughout the following, the white areas indicate locations where model output is not available. These areas are either outside the model domain, such as above ~1×10^{-7} hPa in HAMMONIA, or correspond to time periods that were not included in the model simulation, such as after day 52 (22 February) in WAM. Also note that the WAM model output was only provided above 100 hPa, and results are thus not shown below this altitude despite the fact that WAM does simulate the entire troposphere. When interpreting the results in Figure 1, as well as subsequent figures, it is important to recognize that the models are constrained using different approaches and over different altitude regions. This information is summarized in Table 1, and the results presented herein should be considered in the context of the different model constraints. In Figure 1, the descent of the stratopause beginning around day 15, and the subsequent warming of the stratosphere is clearly seen in the model simulations and the observations. Details of the stratopause descent differ among the models; however, the general features are consistent among all model simulations. The Aura MLS observations reveal a mesospheric cooling associated with the SSW. This feature is generally reproduced by the HAMMONIA, WAM, and WACCM-X simulations, and is very weak in the GAIA simulations. As seen in the Aura MLS observations, an elevated stratopause occurred starting shortly after day 30. The stratopause remained near ~0.01 hPa until the end of February and only descended slightly during this time period. The GAIA, HAMMONIA, and WACCM-X simulations all produce an elevated stratopause. However, WACCM-X is the only simulation that maintains the stratopause height near ~0.01 hPa until the end of February, which is consistent with the observations. The stratopause altitude in the HAMMONIA and GAIA simulations is lower than the observations by the end of February, indicating a faster rate of descent in these simulations. The fact that WACCM-X is the only model to maintain the stratopause at high altitudes until the end of February is thought to be connected to the fact that WACCM-X is nudged to significantly higher altitudes than the other models.

The daily zonal mean zonal wind at 60°N is shown in Figure 2. From Figure 2, it is apparent that the general features of the SSW are reproduced in the stratosphere for all of the models. For example, all of the models

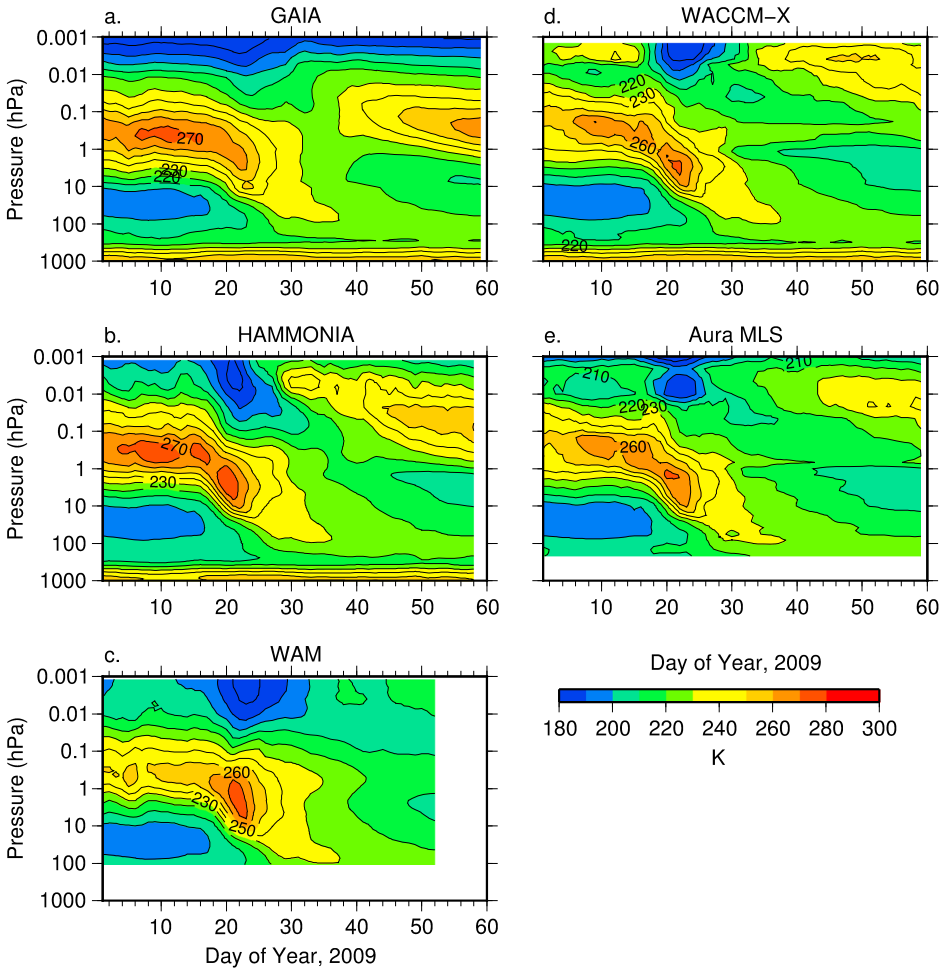

Figure 1. Zonal mean temperature averaged between 70° and 80°N for (a) GAIA, (b) HAMMONIA, (c) WAM, (d) WACCM-X, and (e) Aura MLS.

reveal a reversal of the zonal mean zonal winds near 1 hPa on 20 January and a subsequent descent of the westward winds over the next 5–10 days. The timing of the reversal back to the climatological eastward zonal mean zonal winds near 1–0.1 hPa is also similar among the models. Despite the similarities, notable differences are also evident in Figure 2. Differences among the models are most apparent at higher altitudes where, with the exception of WACCM-X which is constrained up to 0.002 hPa, the models are no longer directly constrained by either data assimilation or reanalysis. When considering the differences in the upper stratosphere and mesosphere, it is important to note that the WACCM-X results are reflective of the merged NOGAPS-ALPHA/MERRA reanalysis, while GAIA, HAMMONIA, and WAM simulations reflect variability that represents a combination of model climatology, internal dynamics, and coupling to the lower atmosphere.

Table 1. The Method Used for Constraining the Lower Model Levels, Along With the Altitude Range of the Constraint

Model	Method of Constraint	Range
GAIA	Nudge to JRA-25 Reanalysis	Surface to 12 hPa
HAMMONIA	Nudge to ECMWF Reanalysis	850 to 1 hPa
WACCM-X	Nudge to NOGAPS-ALPHA/MERRA Reanalysis	Surface to 0.002 hPa
WAM	NOAA Grid point Statistical Interpolation 3D-Var	Surface to 0.1 hPa[a]

[a]WAM only assimilates standard lower atmosphere observations, and the data assimilation thus only directly influences the model up to ~0.1 hPa.

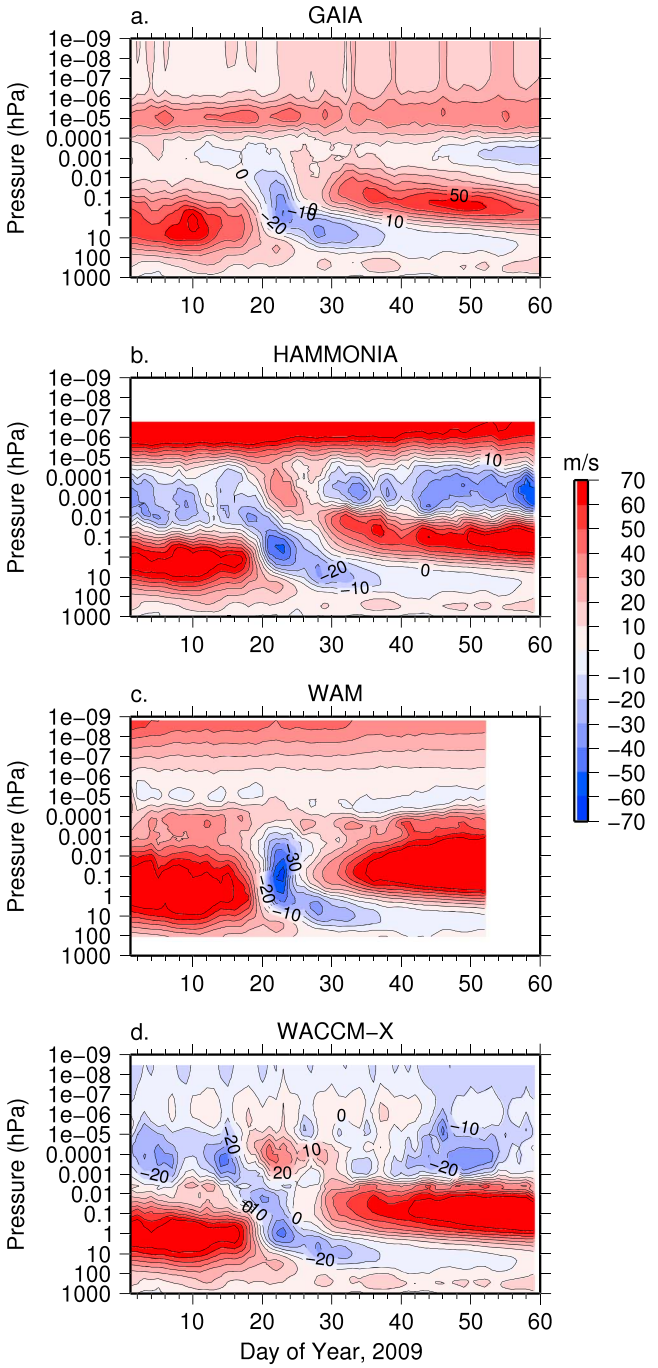

Figure 2. Zonal mean zonal wind at 60°N for (a) GAIA, (b) HAMMONIA, (c) WAM, and (d) WACCM-X.

A clear difference is evident near ~1 hPa, where the models simulate different strengths of the stratospheric eastward winds prior to, and after the SSW. Furthermore, there is a considerable difference among the models in the MLT, with the HAMMONIA and WACCM-X simulations revealing a reversal of the zonal mean zonal winds from westward to eastward near 1×10^{-3} to 1×10^{-5} hPa. The mesospheric reversal coincides with the reversal of the zonal mean zonal winds in the stratosphere. This feature is not present in the GAIA or WAM simulations.

Though there are similarities among the models, the differences in Figure 2 clearly illustrate that there is considerable uncertainty in the model response to the 2009 SSW, especially in the mesosphere and

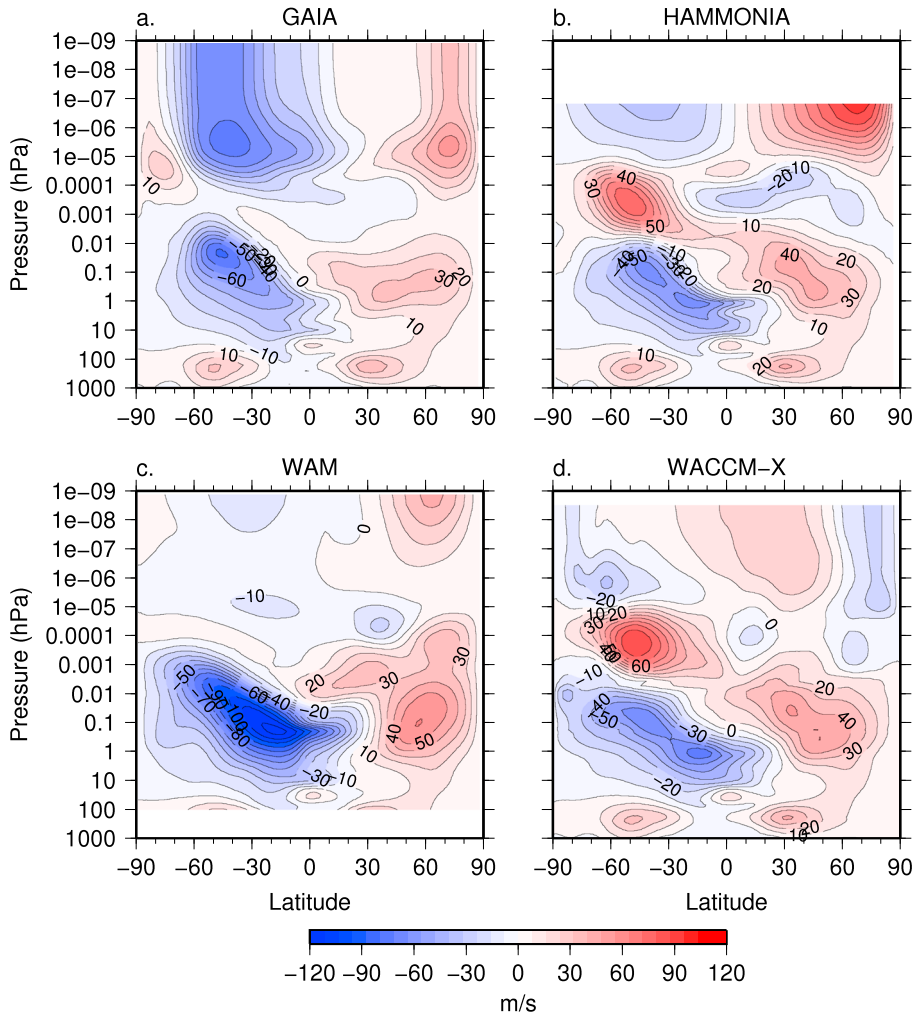

Figure 3. Zonal mean zonal wind averaged from 1 January to 20 February for (a) GAIA, (b) HAMMONIA, (c) WAM, and (d) WACCM-X.

thermosphere. To aid in understanding the source of the differences, Figure 3 shows the simulated zonal mean zonal wind averaged from 1 January to 20 February. The 2009 winter mean results in Figure 3 provide insight into the Northern Hemisphere winter zonal mean zonal wind climatology of the different models; however, it should be noted that due to the long lasting nature of the 2009 SSW, the zonal mean zonal winds presented in Figure 3 should not be taken as equivalent to a multiyear mean climatology. General features, such as eastward winds in the Northern Hemisphere stratosphere and mesosphere, and westward winds in the Southern Hemisphere, are present in all four models. However, the strength of the winter mean stratospheric winds are slightly different among the models. HRDI/WINDII observations by *McLandress et al.* [1996] reveal maximum eastward winds of ~50 ms^{-1} in the Northern Hemisphere and westward winds of ~60 ms^{-1} in the Southern Hemisphere. With the exception of the strong Southern Hemisphere westward winds in WAM, all of the models are thus generally consistent with the observations, especially considering possible effects of interannual variability on the observations and effects of the 2009 SSW on the results in Figure 3. At higher altitudes, there are notable differences in the simulated winter mean zonal mean zonal winds. For example, a clear mesospheric wind reversal is present in HAMMONIA and WACCM-X, only weakly apparent in GAIA, and is only present in the Northern Hemisphere of WAM. The overall features of the mesospheric wind reversal in HAMMONIA, WACCM-X, and the Northern Hemisphere of WAM are generally consistent with HRDI/WINDII observations [*McLandress et al.*, 1996]. Given that there are some considerable differences in the January-February average zonal mean zonal wind, it is not surprising that there is disagreement among the model simulated zonal mean zonal winds during the 2009 SSW.

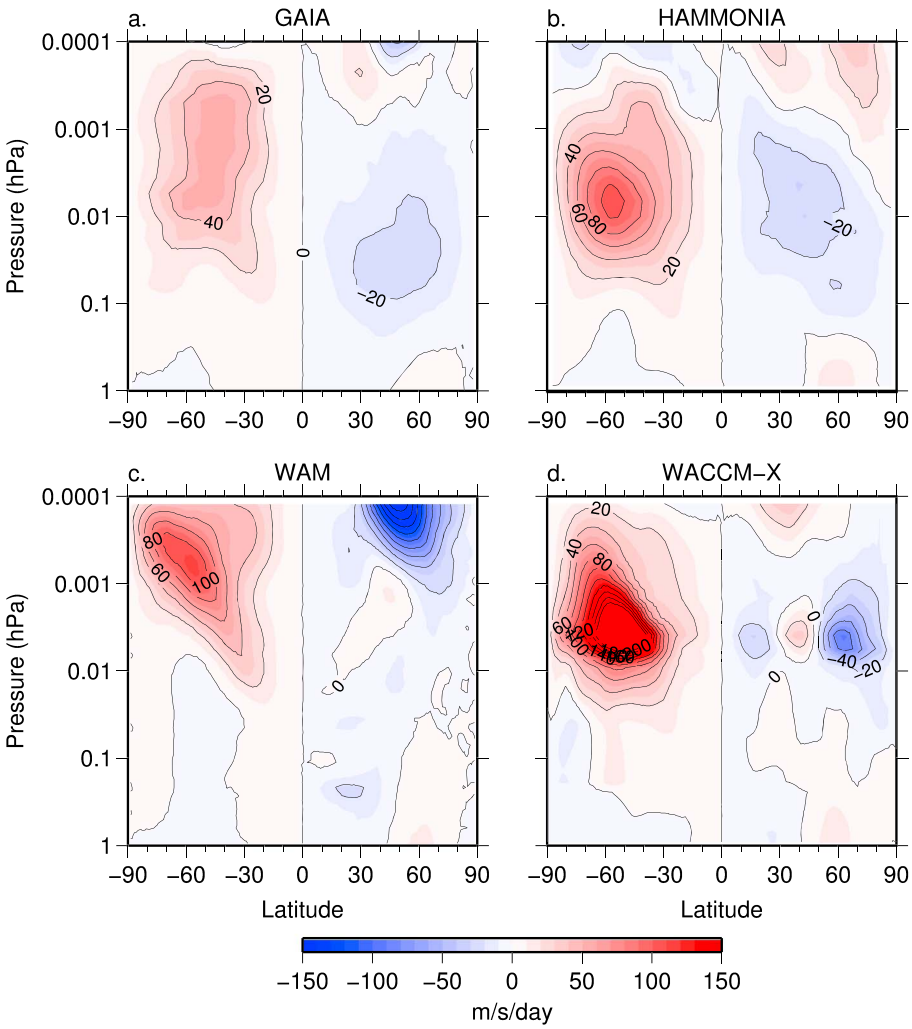

Figure 4. Zonal mean gravity wave forcing derived from momentum balance averaged from 1 January to 20 February for (a) GAIA, (b) HAMMONIA, (c) WAM, and (d) WACCM-X.

It is well understood that the breaking of gravity waves is a fundamental driver of the circulation in the stratosphere, mesosphere, and lower thermosphere [*Garcia and Solomon*, 1985; *Alexander et al.*, 2010]. Gravity wave drag parameterizations are thus critical for correctly modeling the middle atmosphere circulation, and the gravity wave drag parameterizations are typically tuned so that the model climatology is consistent with observations. We therefore anticipate that differences in gravity wave drag parameterizations are significantly contributing to the differences in the simulated zonal mean zonal winds during the 2009 SSW. To examine differences in the gravity wave drag, the zonal mean gravity wave forcing is estimated using the momentum balance relationship. Following *Liu et al.* [2009], the zonal mean gravity wave forcing is calculated as

$$\bar{F}_x^{GW} = -\left(f + \frac{\bar{u}\tan\phi}{r}\right)\bar{v} \tag{1}$$

where f is the Coriolis parameter, r the Earth radius, ϕ latitude, and u and v the zonal and meridional winds, respectively. The overbars in (1) denote zonal mean parameters. It should be noted that the gravity wave forcing calculated from (1) is an approximation that is only valid at MLT altitudes. The zonal mean gravity wave forcing averaged from 1 January to 20 February is shown in Figure 4. Similar to the zonal mean zonal winds, the general features of the zonal mean gravity wave forcing are similar among the different models. However, the amplitudes of the zonal mean gravity wave forcing differ significantly among the models. In the MLT, we attribute a significant portion of the differences in both the winter mean zonal mean zonal winds and the zonal mean zonal wind variability during the 2009 SSW to be due to the differences in the

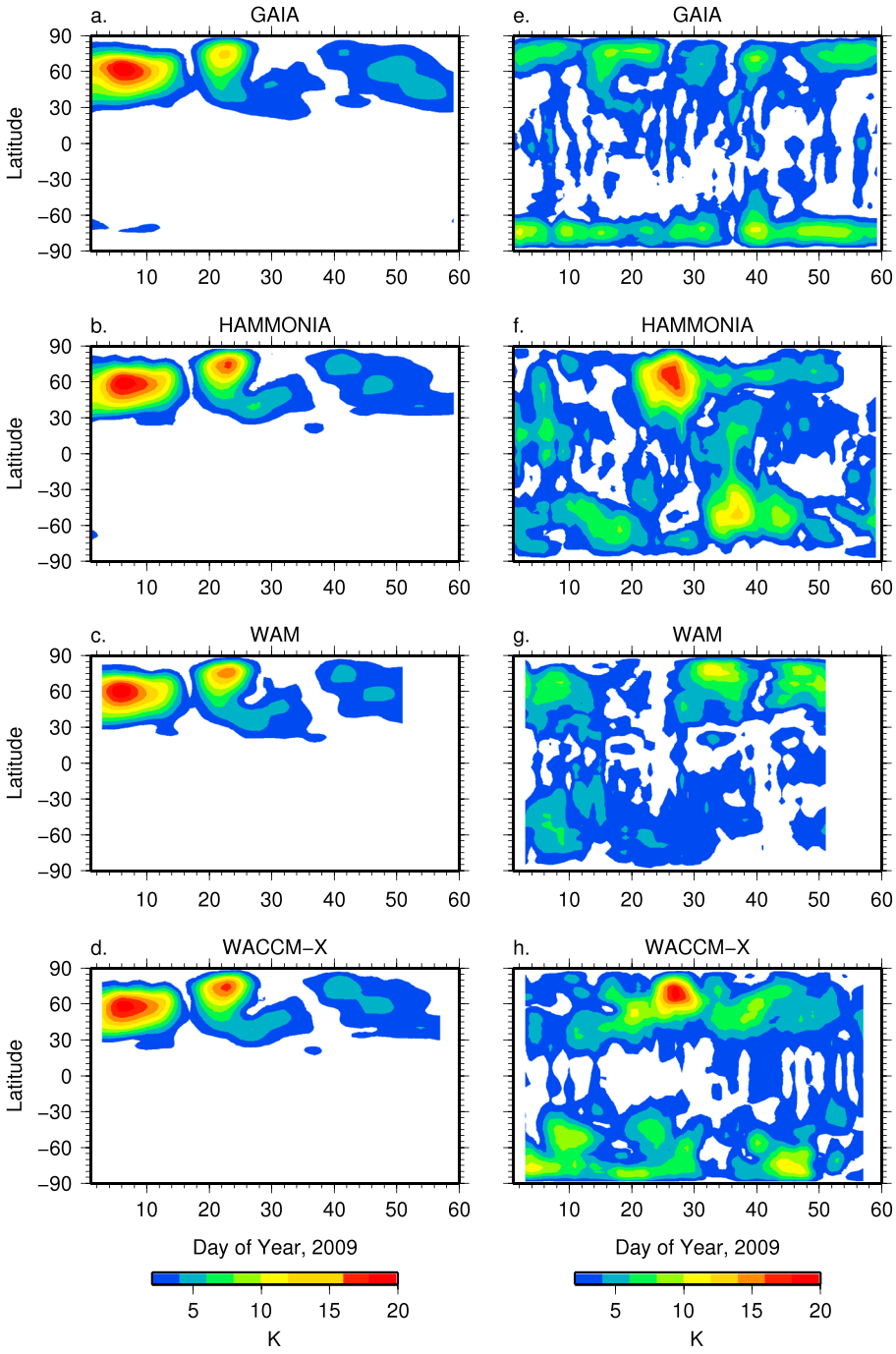

Figure 5. Planetary wave 1 amplitude of temperature at 10 hPa (~30 km) for (a) GAIA, (b) HAMMONIA, (c) WAM, and (d) WACCM-X. (e–h) Same as Figures 5a–5d except for at 1×10^{-4} hPa (~110 km).

gravity wave drag forcing. The differences in the gravity wave forcing, and the subsequent impact on the zonal mean variability, demonstrate the importance of the gravity wave drag parameterizations on reliably simulating the middle and upper atmosphere variability during SSWs. This is especially the case at altitudes where the models are unconstrained. In the absence of direct constraint by data assimilation or nudging, the variability that occurs in the MLT is primarily coupled to changes in the lower atmosphere through gravity wave drag parameterizations [e.g., *McLandress et al.*, 2013]. Developing adequate gravity wave drag parameterizations is therefore considered to be of utmost importance for accurately simulating the dynamical variability that occurs during SSWs.

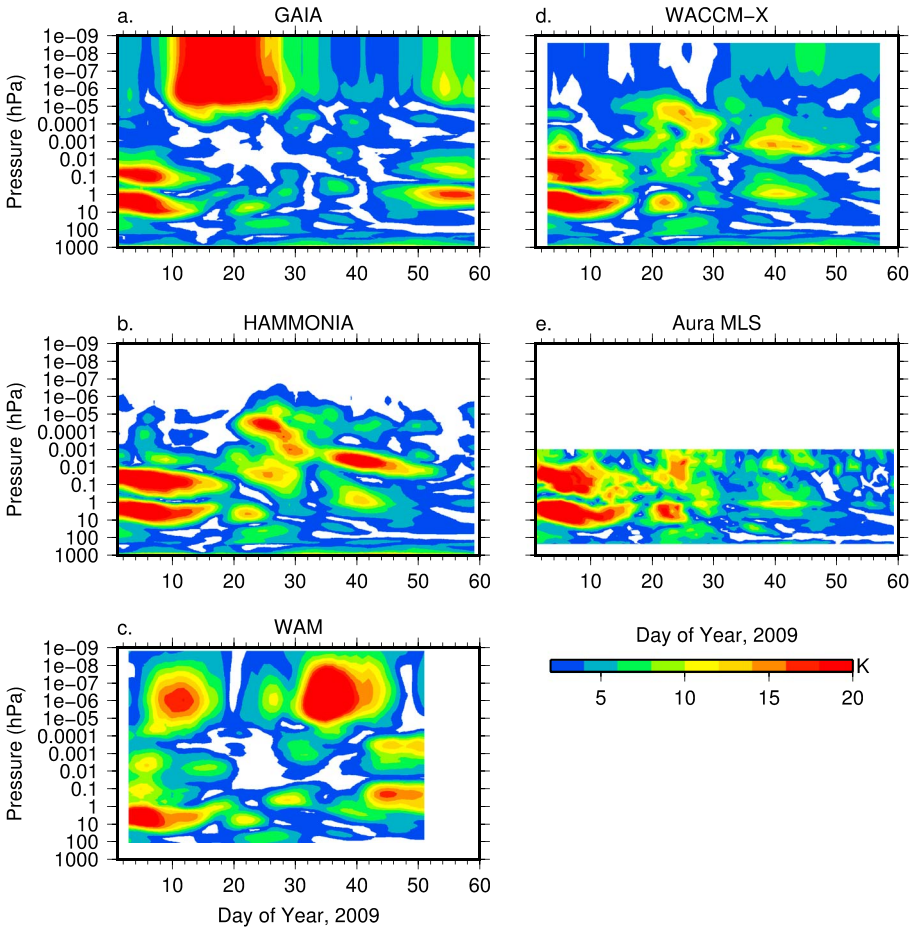

Figure 6. Planetary wave 1 amplitude of temperature at 60°N for (a) GAIA, (b) HAMMONIA, (c) WAM, (d) WACCM-X, and (e) Aura MLS observations.

3.2. Planetary Wave Variability

Enhanced nonmigrating tides that are generated through nonlinear planetary wave-tide interactions is one potential mechanism for coupling SSWs to disturbances in the ionosphere [e.g., *Liu et al.*, 2010a; *Pedatella and Forbes*, 2010]. The planetary wave variability in the model simulations of the 2009 SSW is therefore considered to be important for impacting SSW-ionosphere coupling. Furthermore, the simulated variability at MLT altitudes provides insight into potential differences among the models in terms of the vertical propagation of waves from the stratosphere to the MLT. Figure 5 shows the amplitude of planetary wave 1 (*PW*1) in temperature at 10 hPa and 1×10^{-4} hPa. Though there are some minor differences, the simulated *PW*1 at 10 hPa is similar among all four models. The models all simulate enhanced *PW*1 at high latitudes in the Northern Hemisphere with maxima centered on days 6 and 23. An additional enhancement beginning on day 40 is also evident in all of the model simulations. In addition to exhibiting similar temporal variability, the model simulations are also in agreement in terms of the *PW*1 amplitude at 10 hPa. This demonstrates that all of the models are in good agreement in the stratosphere, providing a verification that the different methods for constraining the lower atmosphere yield consistent results at lower altitudes where their dynamics are well constrained.

Similar to the zonal mean variability, Figures 5e–5h illustrate that there is significantly less agreement among the models at higher altitudes for the *PW*1. All four models exhibit considerable temporal variability in the *PW*1 at 1×10^{-4} hPa (~110 km); however, there is little agreement among the models in terms of the timing of the enhancements. It is important to note that 1×10^{-4} hPa is above where the models are constrained, and the simulated *PW*1 variability at this altitude thus occurs due to internal model dynamics (i.e., it is not imposed on the model through data assimilation or nudging toward reanalysis). Since the *PW*1 is similar in the stratosphere, the differences in the *PW*1 at MLT altitudes are thus considered to be due

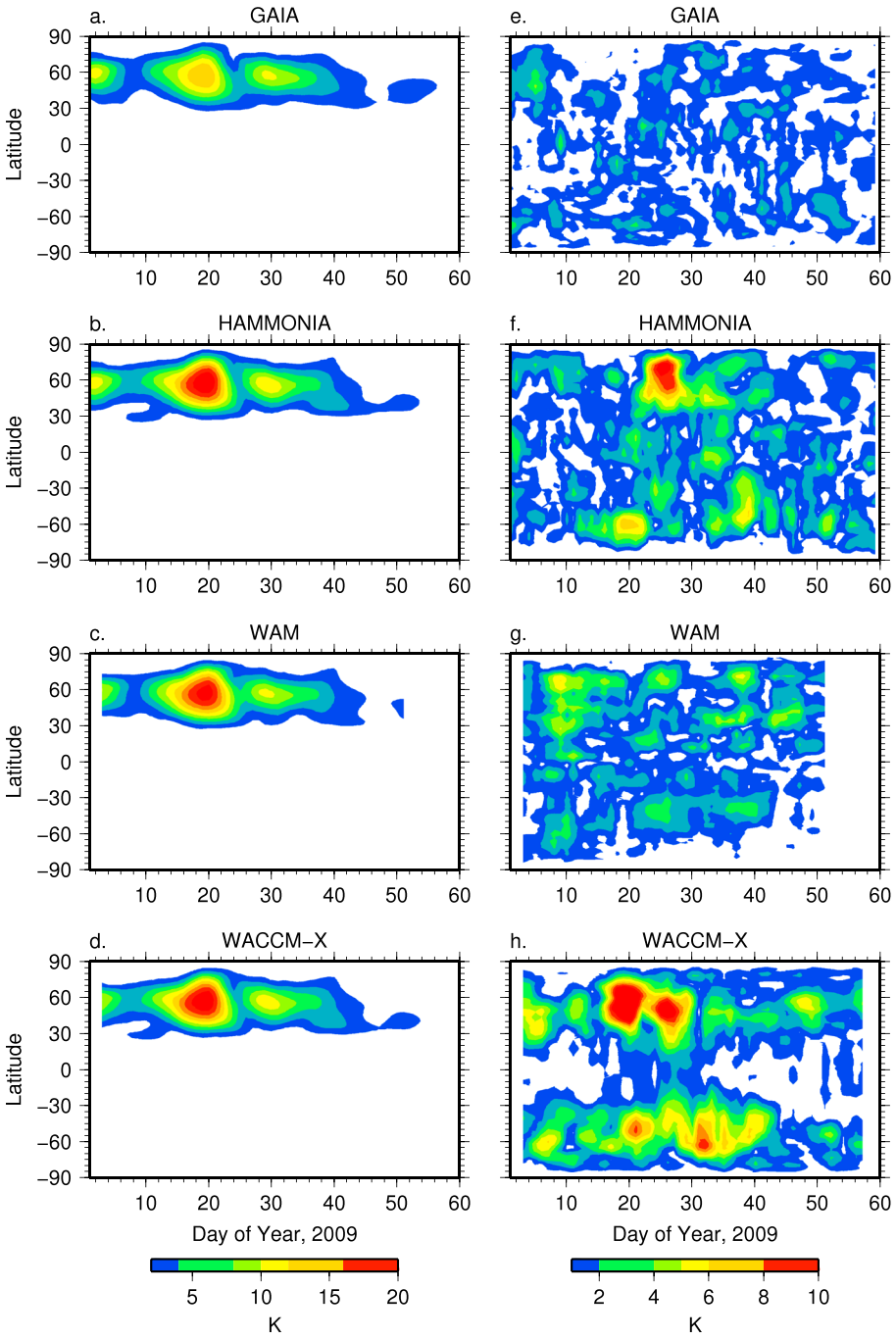

Figure 7. Same as Figure 5 except for planetary wave 2.

to differences in the vertical propagation from lower altitudes combined with in situ forcing by breaking gravity waves [e.g., *Smith*, 2003]. We therefore attribute the differences in the *PW*1 at MLT altitudes to be primarily due to differences in the simulated zonal mean zonal winds and the gravity wave drag parameterizations. This is supported by the fact that the *PW*1 variability in the MLT is generally similar in HAMMONIA and WACCM-X, and the simulated zonal mean zonal winds are similar in these two models. As previously discussed, the zonal mean zonal wind differences can be traced back to differences in the gravity wave drag parameterizations. This demonstrates that the gravity wave drag parameterizations are important not only for the zonal mean circulation but also for accurately modeling the planetary wave variability during SSWs.

The evolution of the *PW*1 in temperature with height is shown in Figure 6, which shows the *PW*1 amplitude at 60°N. For comparison, the amplitude of the *PW*1 in temperature observed by Aura MLS is shown in Figure 6e. It is again apparent that the models are in good agreement up to ~10 to 1 hPa and that above this altitude the models begin to diverge significantly. In general, the model simulations capture the major enhancements in the *PW*1 observed by Aura MLS. For example, the double peaked structure that occurs from days 1 to 10 is present in all of the model simulations, though the maximum at higher altitudes is weak in the WAM simulation. The Aura MLS observations also reveal weaker enhancements from days 20 to 25 and around day 40. Aspects of these weaker enhancements can be seen in the different model simulations; however, they are not as well reproduced compared to the enhancement that occurred during early January.

The 2009 SSW was a wave 2 event, involving a splitting of the polar vortex. Planetary wave 2 (*PW*2) was thus large in the time period preceding the 2009 SSW. Figure 7 shows the amplitude of *PW*2 in temperature at 10 hPa and 1×10^{-4} hPa. Consistent with the results for *PW*1, all four models simulate similar variability in the *PW*2 at 10 hPa, with enhancements occurring at high latitudes in the Northern Hemisphere on days 2, 19, and 29. The maximum amplitude of the enhancements are generally similar among the model simulations; however, the amplitude of the enhancement on day 19 in GAIA is ~5 K less than what is simulated by HAMMONIA, WAM, and WACCM-X. At MLT altitudes (Figures 7e–7h), although all of the models display considerable *PW*2 variability, there is little agreement among the models in terms of the *PW*2. The evolution of the *PW*2 with height is shown in Figure 8, which shows the *PW*2 amplitude at 60°N, along with the Aura MLS observations (Figure 8e). The dominant feature of the observations is the large enhancement that occurs from days 18 to 20. This enhancement is well reproduced in all of the model simulations. We again note that although the model simulations are similar at lower altitudes, the models begin to diverge significantly in the mesosphere. This is again attributed to the differences in the zonal mean atmosphere, and gravity wave drag parameterizations, which will impact the propagation of the *PW*2 from the stratosphere into the MLT.

3.3. Migrating and Nonmigrating Tides

Though the exact mechanisms are yet to be fully understood, it is now generally accepted that the modulation of atmospheric tides during SSWs is the primary mechanism for coupling between SSWs and ionosphere variability [*Chau et al.*, 2012]. The ability of whole atmosphere models to accurately simulate the variability in atmospheric tides is thus critical for simulating, and potentially predicting, the ionosphere response to SSWs. Given the importance of the tidal variability during SSWs, and the lack of observations for comparison, it is important to compare the model simulated tides in order to gain a sense of the consistency of the simulated tidal response to the 2009 SSW. Figure 9 shows the amplitude and phase of the migrating diurnal tide (*DW*1) at 0.01 hPa (~80 km). In the equatorial region, all four models simulate an amplitude enhancement maximizing on day 15 of 7–8 K, followed by a decrease in amplitude, and then a gradual increase in the *DW*1 amplitude until the end of February (day 60). The models also all indicate that the *DW*1 phase decreases by ~6 h at equatorial latitudes beginning around day 20, though this phase shift is slightly less in the GAIA simulation. The phase gradually increases back toward pre-SSW values following the SSW peak. The agreement in both amplitudes and phases demonstrates that the models are generally consistent in terms of the temporal variability of the *DW*1 before, during, and after the 2009 SSW. The consistency among the model simulations is an important result and illustrates that despite the use of different model parameterizations and methods for constraining the lower atmosphere, different models can obtain a similar result for the MLT tidal variability.

The *SW*2 can significantly impact the ionosphere electrodynamics [e.g., *Fesen et al.*, 2000], and the model simulated *SW*2 during SSWs is thus of critical importance for reproducing the ionosphere perturbations during SSWs. The simulated amplitudes and phases of the *SW*2 at $1\text{x}10^{-4}$ hPa (~110 km) are shown in Figure 10. Compared to the *DW*1, there is significantly less agreement among the models for the *SW*2. The discrepancy in the simulated *SW*2 is particularly evident for the *SW*2 amplitudes. The amplitude maxima are ~45 K, ~30 K, ~80 K, and ~15 K in GAIA, HAMMONIA, WAM, and WACCM-X, respectively. There is thus considerable uncertainty in terms of the simulated *SW*2 amplitude during the 2009 SSW. The *SW*2 amplitude differences may stem from different treatments of ozone variability, which may be an important driver of *SW*2 variability during SSWs [*Goncharenko et al.*, 2012]. Alternatively, *Jin et al.* [2012] attributed the *SW*2 variability during the 2009 SSW to be due to changes in the zonal mean zonal winds, and the differences in the simulated *SW*2 amplitudes could be due to the different simulated zonal mean zonal winds. The weak *SW*2 in WACCM-X may be related to specific model parameterizations, or the vertical resolution, which result in an underestimation of tidal amplitudes in WACCM [e.g., *Liu et al.*, 2010b; *Davis et al.*, 2013]. Despite the disagreement in

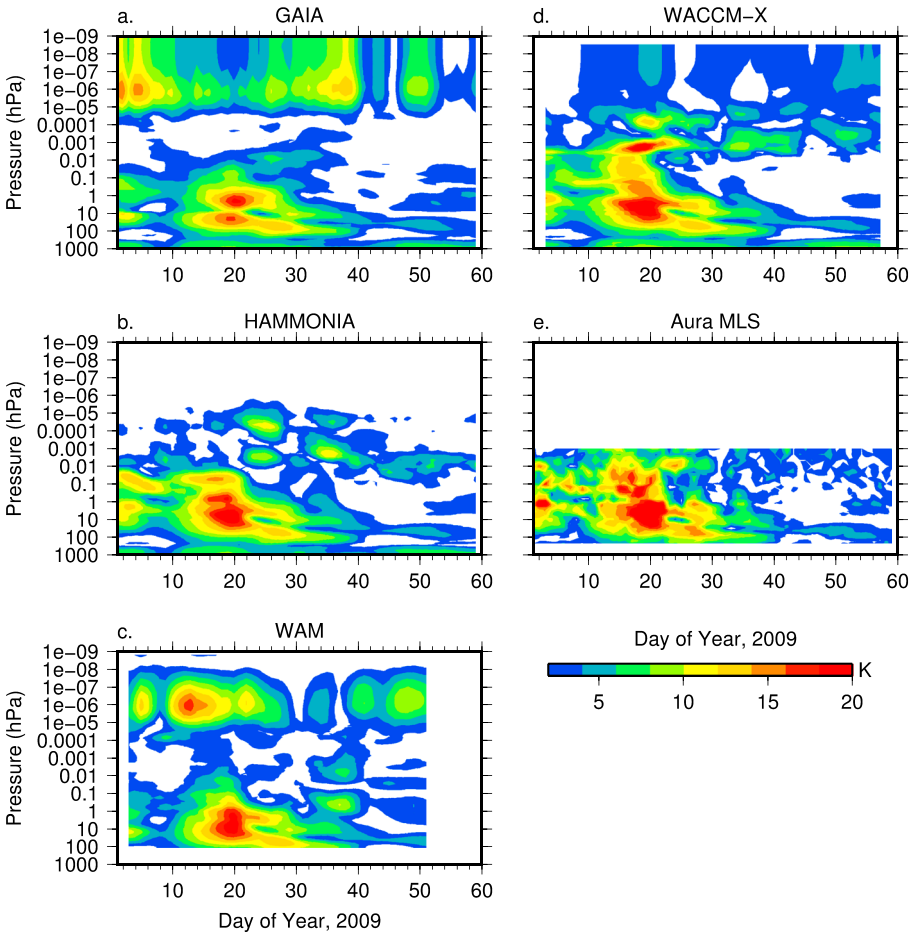

Figure 8. Same as Figure 6 except for planetary wave 2.

terms of the absolute values, the temporal variability of the *SW*2 is consistent among the four models. All of the models reveal a reduction in the *SW*2 amplitude that occurs around days 15–20 and a subsequent enhancement in the *SW*2 amplitude between days 30 and 40. The consistency of the *SW*2 amplitude variability indicates that this is likely reflective of the true *SW*2 temporal evolution that occurred during the 2009 SSW. Though there are some differences, GAIA, HAMMONIA, and WAM all reveal qualitatively similar changes in the *SW*2 phase during the SSW. A clear pattern is not apparent in the WACCM-X phase changes. At midlatitudes, where the *SW*2 maxima occur, the GAIA, HAMMONIA, and WAM simulations all reveal an initial decrease in the *SW*2 phase by several hours, followed by an increase in the *SW*2 phase. A shift in the *SW*2 phase is thought to be important for driving the low latitude ionosphere response to SSWs [*Pedatella and Liu*, 2013]. Furthermore, using COSMIC ionosphere observations, *Lin et al.* [2013] found a decrease in the phase of the *DW*1 and *SW*2 beginning around 15–20 January 2009. Though tidal phase variations in the MLT may not directly correspond to phase variations in the ionosphere, the consistent behavior of the model simulations and the observations in terms of the *DW*1 and *SW*2 phase variability is encouraging for reliably reproducing the ionosphere response.

The semidiurnal westward propagating nonmigrating tide with zonal wavenumber 1 (*SW*1) amplitudes and phases are shown in Figure 11 at 1×10^{-4} hPa. The *SW*1 can also influence the ionosphere electrodynamics [*Liu and Richmond*, 2013], and it is thus important to assess the capabilities of the models to reproduce the *SW*1 variability. Though all four models indicate significant day-to-day variability in the *SW*1, there does not appear to be any clear agreement in the simulation results for the *SW*1. The lack of agreement in the *SW*1 may be expected based on the previously presented results. The *SW*1 is primarily generated by the nonlinear interaction of the *PW*1 and *SW*2 [*Liu et al.*, 2010a]. Given the notable differences in the *PW*1 at MLT

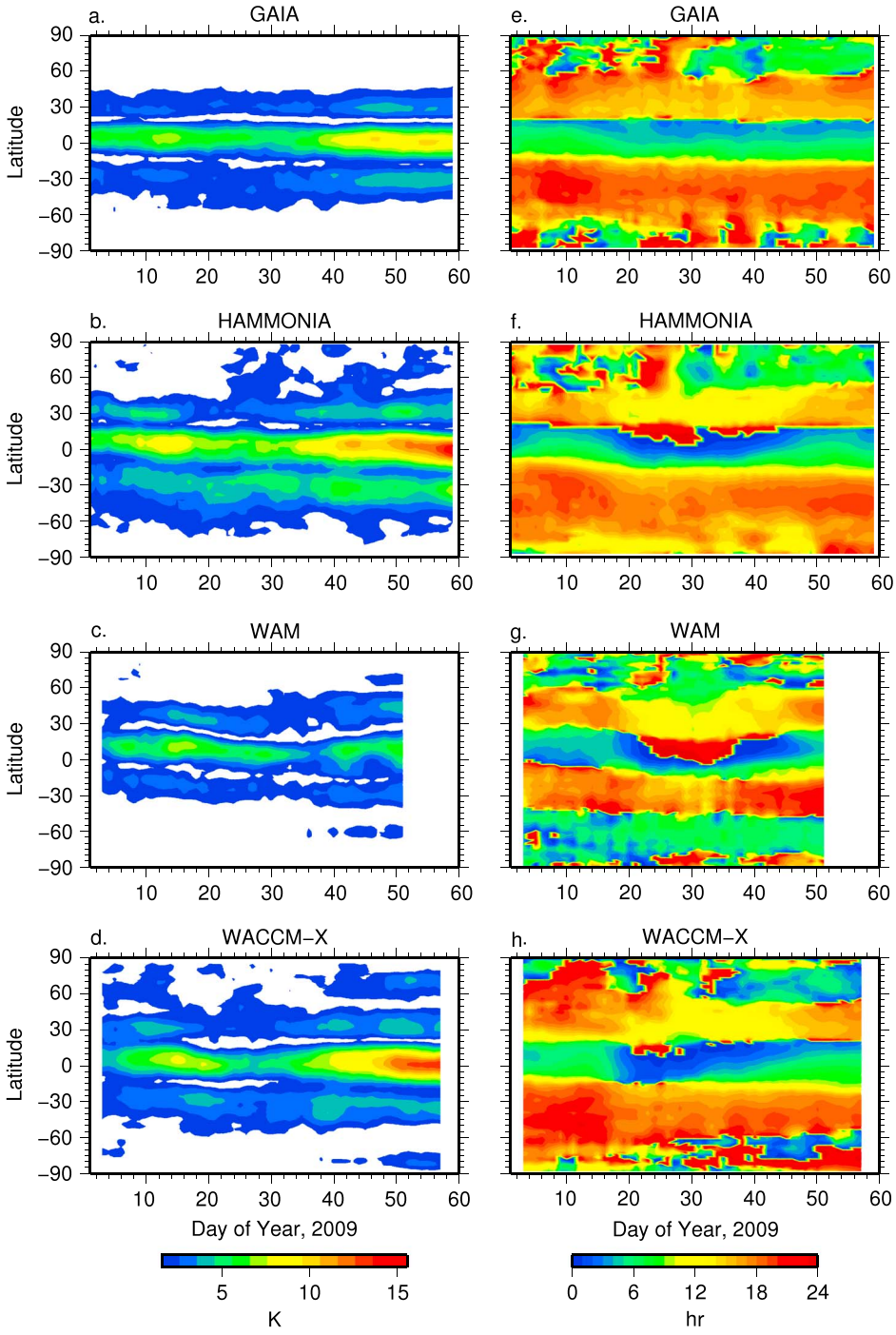

Figure 9. *DW*1 amplitude of temperature at 0.01 hPa (~80 km) for (a) GAIA, (b) HAMMONIA, (c) WAM, and (d) WACCM-X. (e–h) Same as Figures 9a–9d except for the *DW*1 phase.

altitudes (Figures 7 and 8), it is not surprising that there is little agreement for the *SW*1. Since *SW*1 is a non-migrating tide, and therefore is longitudinally dependent at a fixed local time, the considerable differences in the simulated *SW*1 may have consequences for the simulated local time variability at specific longitudes. Results for the *SW*1 demonstrate that there are aspects of the modeled tidal response to the 2009 SSW that are significantly different among the models, and that portions of the middle and upper atmosphere response to SSWs are highly uncertain in the model simulations.

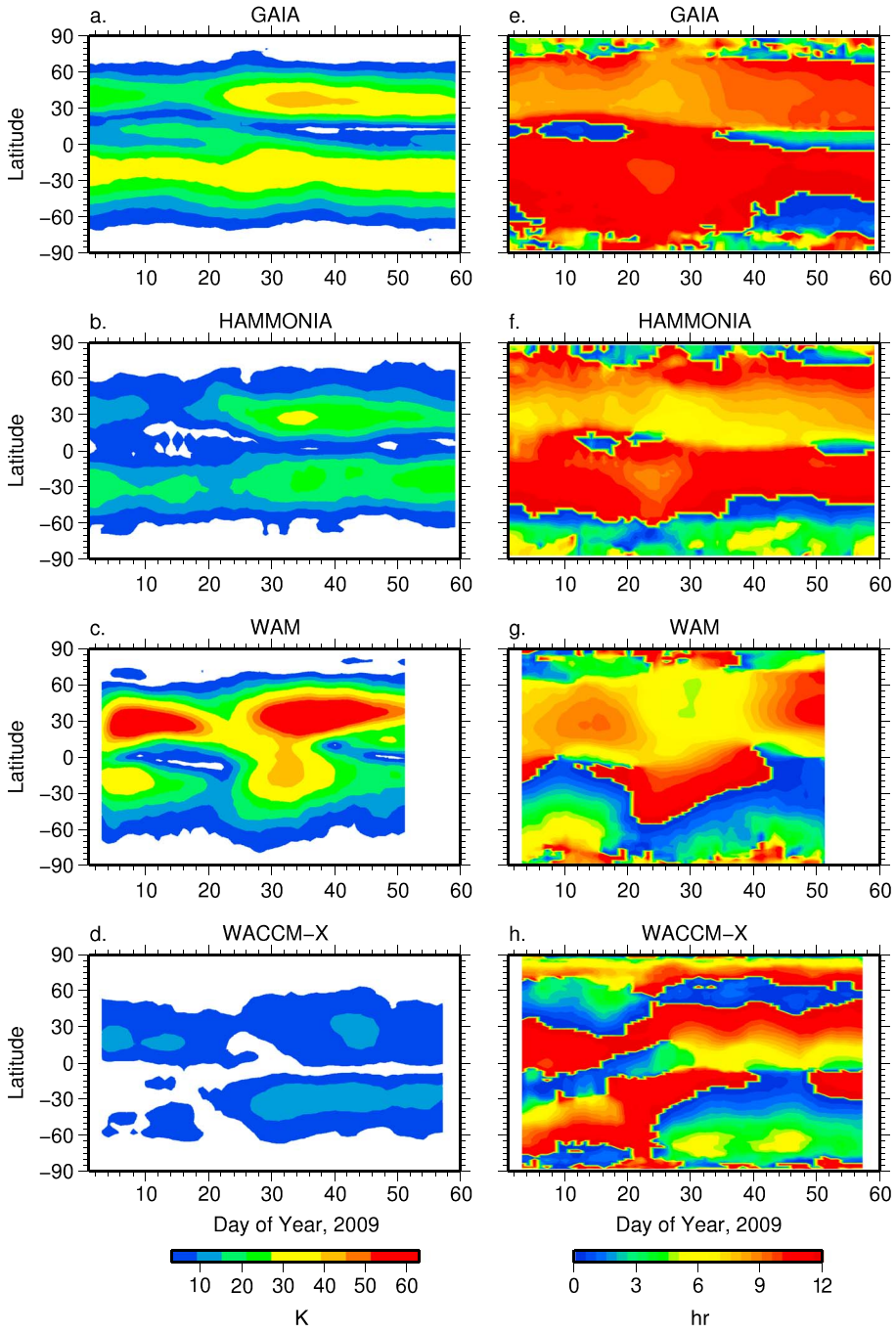

Figure 10. *SW*2 amplitude of temperature at 1×10^{-4} hPa (~110 km) for (a) GAIA, (b) HAMMONIA, (c) WAM, and (d) WACCM-X. (e–h) Same as Figures 10a–10d except for the *SW*2 phase.

4. Summary and Conclusions

Recent developments in whole atmosphere modeling have enabled realistic simulations of the atmospheric response to SSWs from the surface to the upper thermosphere. Model simulations of SSWs not only are important for understanding the variability throughout the atmosphere during SSWs but also are potentially useful for predicting upper atmosphere variability by running in a forecast mode. Verifying the simulation results in the middle and upper atmosphere has, however, remained difficult owing to the lack of global-scale observations with sufficient temporal resolution. The accuracy of the simulations in the middle and upper atmosphere is thus largely unknown, and this is especially true for the short-term variability.

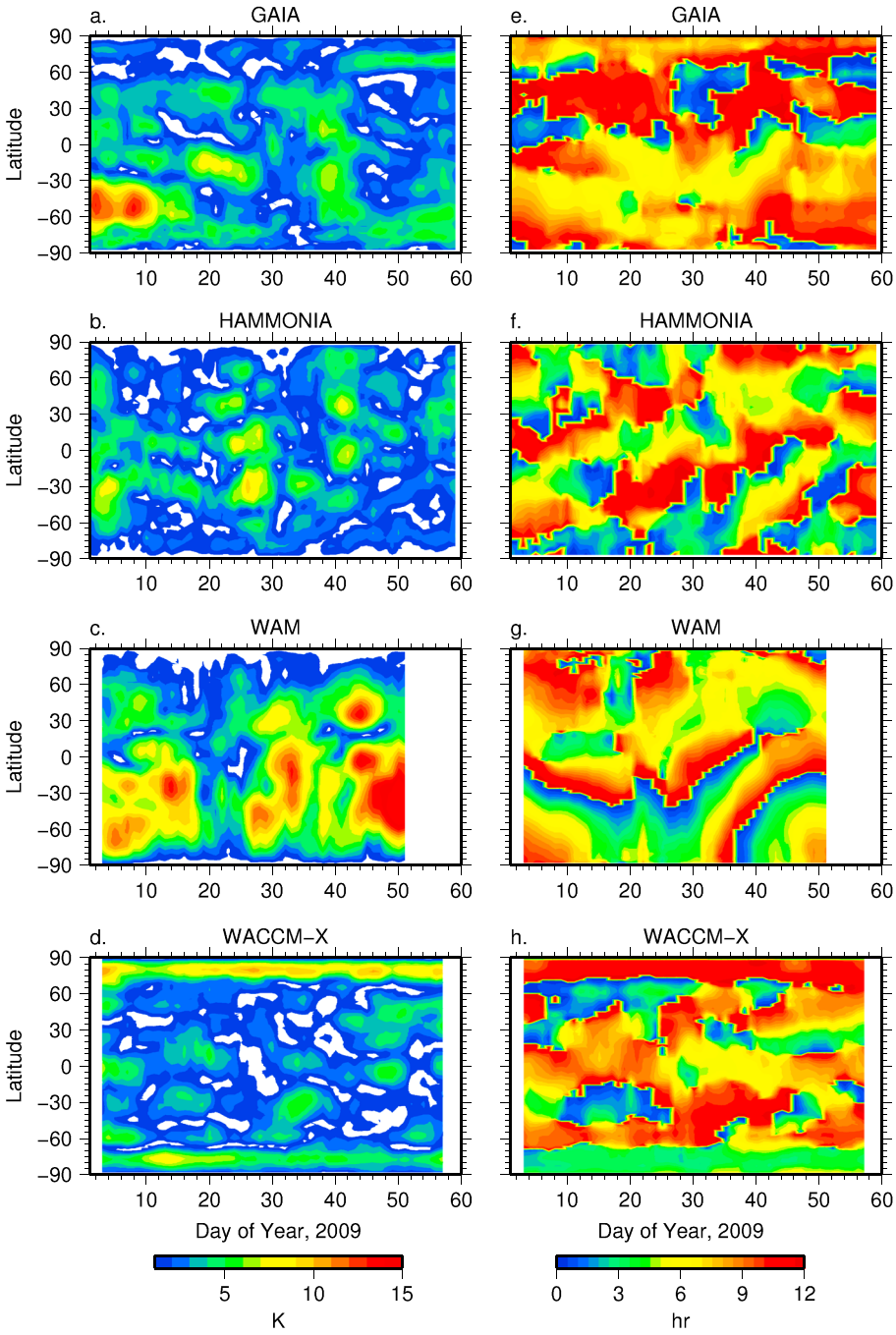

Figure 11. *SW*1 amplitude of temperature at 1x10^{-4} hPa (~110 km) for (a) GAIA, (b) HAMMONIA, (c) WAM, and (d) WACCM-X. (e–h) Same as Figures 11a–11d except for the *SW*1 phase.

In the present study, we have compared four different whole atmosphere model simulations of the 2009 SSW to gain insight into the similarities, and differences, of the zonal mean, planetary wave, and tidal variability. The comparison provides a useful sense of how confident one should be in aspects of the model simulations. Our conclusions are summarized as follows:

1. Above ~1 hPa, significant differences are found in the zonal mean zonal wind and temperature that is simulated by the four models. GAIA, HAMMONIA, and WACCM-X all reproduce the elevated stratopause that occurs in the Aura MLS observations following the SSW. However, the stratopause descends too fast in the GAIA and HAMMONIA simulations, and WACCM-X is the only model that maintains the stratopause

near 0.01 hPa until the end of February. The zonal mean zonal wind differences during the SSW are partly related to notable differences in the Northern Hemisphere wintertime average zonal mean zonal winds. We attribute the differences in the zonal mean zonal winds to be the consequence of differences in the gravity wave drag parameterizations.

2. Variability in stratospheric planetary waves, which are responsible for generating the SSW, is similar among all of the models. This illustrates that the different approaches used to constrain the lower atmosphere are consistent in terms of their ability to constrain the troposphere and stratosphere. The model simulations generally reproduce the dominant features of the planetary wave variability in the Aura MLS observations. The evolution of the planetary waves with height is significantly different among the models leading to large differences in the planetary waves at MLT altitudes. The notable differences in the planetary wave variability in the MLT is thought to be due to differences in the in situ forcing by breaking gravity waves and effects of the different zonal mean zonal winds on the vertical propagation.
3. Analysis of migrating and nonmigrating tides in the MLT during the 2009 SSW yields mixed results. The amplitude and temporal evolution of the *DW*1 is similar among all of the model simulations. All four models also simulate similar temporal variations in the *SW*2 amplitude, although there are significant differences in the absolute *SW*2 amplitudes. Results for the *DW*1 illustrate consistent phase variability among all of the simulations, and the *SW*2 phase variability is also consistent among GAIA, HAMMONIA, and WAM. No clear agreement is found for the *SW*1.

It is important to note that modeling capabilities are continually improving. The results presented herein are representative of the current modeling capabilities, and future model improvements will likely lead to improved consistency among the model results. Model improvements are also likely to result in improved agreement with observations, i.e., more realistic simulations. A particular area that should be the focus of future development is the parameterization of gravity wave drag. Our results illustrate the importance of gravity wave drag parameterizations for accurately simulating the middle and upper atmosphere response to SSWs. In addition to influencing the zonal mean circulation, the gravity wave drag parameterizations indirectly impact the planetary wave and tidal variability in the MLT due to the effects of the zonal mean atmosphere on upward propagating planetary waves and tides. Gravity wave drag parameterizations are thus an extremely important aspect of simulating the middle and upper atmosphere response to SSWs and should be a focus of future model developments. Last, it is our intention that the model comparison performed in the present study can be used as a guide toward what aspects should be considered as robust features of the MLT response to SSWs, as well as those features that should be considered as highly uncertain. The level of uncertainty in the middle and upper atmosphere response is often neglected, and the present study highlights that this is important to consider owing to the potentially significant uncertainty in certain aspects of the simulations.

Acknowledgments

We acknowledge support from the International Space Science Institute for facilitating the discussions leading to the present model comparison. The National Center for Atmospheric Research is sponsored by the National Science Foundation. This work was supported in part by a NCAR Advanced Study Program Postdoctoral Fellowship (N.P.). H.L. acknowledges support from NSF grant AGS-1138784. F.S. and H.L. were partially supported by NASA/LWS grant NNH12AT21L. In addition, F.S. was also supported by ONR 6.1 base funding. WACCM-X simulations were supported by a grant of computer time from the DoD High Performance Computing Modernization Program at the US Navy DoD Supercomputing Resource Center (NAVO). We thank Fei Wu for providing the output from the WAM simulation used in the analysis and Rashid Akmaev for helpful discussions. This work was supported at the University of Colorado in part by NASA Heliophysics Theory Grant NNX11AO61G and NASA LWS Strategic Capabilities grant NX09AJ83G. L.G. has been supported through NSF grant AGS-1132267 and NASA LWS grant NNX13AI62G. The meteorological reanalysis data used in the GAIA simulation are provided from the cooperative research project of the JRA-25 long-term reanalysis by the Japan Meteorological Agency (JMA) and the Central Research Institute of Electric Power Industry (CRIEPI).

Robert Lysak thanks Christoph Zuelicke and an anonymous reviewer for their assistance in evaluating this paper.

References

Akmaev, R. A. (2011), Whole atmosphere modeling: Connecting terrestrial and space weather, *Rev. Geophys.*, *49*, RG4004, doi:10.1029/2011RG000364.

Akmaev, R. A., T. J. Fuller-Rowell, F. Wu, J. M. Forbes, X. Zhang, A. F. Anghel, M. D. Iredell, S. Moorthi, and H.-M. Juang (2008), Tidal variability in the lower thermosphere: Comparison of Whole Atmosphere Model (WAM) simulations with observations from TIMED, *Geophys. Res. Lett.*, *35*, L03810, doi:10.1029/2007GL032584.

Alexander, M. J., M. Geller, C. McLandress, S. Polavarapu, P. Preusse, F. Sassi, K. Sato, S. Eckermann, M. Ern, A. Hertzog, Y. A. Kawatani, M. Pulido, T. Shaw, M. Sigmond, R. Vincent, and S. Watanabe (2010), Recent developments in gravity-wave effects in climate models and the global distribution of gravity-wave momentum flux from observations and models, *Q. J. R. Meteorol. Soc.*, *136*, 1103–1124, doi:10.1002/qj.637.

Alpert, J. C., M. Kanamitsu, P. M. Caplan, J. G. Sela, G. H. White, and E. Kalnay (1988), Mountain induced gravity wave drag parameterization in the NMC medium-range model, Preprints of the Eighth Conference on Numerical Weather Prediction, pp. 726–733, American Meteorological Society, Baltimore, Md.

Charlton, A. J., and L. M. Polvani (2007), A new look at stratospheric sudden warmings. Part I: Climatology and modeling benchmarks, *J. Clim.*, *20*, 449–469.

Charlton, A. J., A. O'Neill, W. A. Lahoz, and P. Berrisford (2005), The splitting of the stratospheric polar vortex in the Southern Hemisphere, September 2002: Dynamical evolution, *J. Atmos. Sci.*, *62*, 590–602.

Chau, J. L., B. G. Fejer, and L. P. Goncharenko (2009), Quiet variability of equatorial ExB drifts during a sudden stratospheric warming event, *Geophys. Res. Lett.*, *36*, L05101, doi:10.1029/2008GL036785.

Chau, J. L., N. A. Aponte, E. Cabassa, M. P. Sulzer, L. P. Goncharenko, and S. A. González (2010), Quiet time ionospheric variability over Arecibo during sudden stratospheric warming events, *J. Geophys. Res.*, *115*, A00G06, doi:10.1029/2010JA015378.

Chau, J. L., L. P. Goncharenko, B. G. Fejer, and H.-L. Liu (2012), Equatorial and low latitude ionospheric effects during sudden stratospheric warming events, *Space Sci. Rev.*, *168*, 385–417, doi:10.1007/s11214-011-9797-5.

Cho, Y.-M., G. G. Shepherd, Y.-I. Won, S. Sargoytchev, S. Brown, and B. Solheim (2004), MLT cooling during stratospheric warming events, *Geophys. Res. Lett.*, *31*, L10104, doi:10.1029/2004GL019552.

Davis, R. N., J. Du, A. K. Smith, W. E. Ward, and N. J. Mitchell (2013), The diurnal and semidiurnal tides over Ascension Island (8° S, 14° W) and their interaction with the stratospheric QBO: studies with meteor radar, eCMAM and WACCM, *Atmos. Chem. Phys. Discuss.*, *13*, 4785–4837, doi:10.5194/acpd-13-4785-2013.

Fejer, B. G., M. E. Olson, J. L. Chau, C. Stolle, H. Lühr, L. P. Goncharenko, K. Yumoto, and T. Nagatsuma (2010), Lunar-dependent equatorial ionospheric electrodynamic effects during sudden stratospheric warmings, *J. Geophys. Res.*, *115*, A00G03, doi:10.1029/2010JA015273.

Fesen, C. G., G. Crowley, R. G. Roble, A. D. Richmond, and B. G. Fejer (2000), Simulation of the pre-reversal enhancement in the low latitude vertical ion drifts, *Geophys. Res. Lett.*, *27*(13), 1851–1854, doi:10.1029/2000GL000061.

Forbes, J. M., and X. Zhang (2012), Lunar tide amplification during the January 2009 stratosphere warming event: Observations and theory, *J. Geophys. Res.*, *117*, A12312, doi:10.1029/2012JA017963.

Fuller-Rowell, T. J., et al. (2008), Impact of terrestrial weather on the upper atmosphere, *Geophys. Res. Lett.*, *35*, L09808, doi:10.1029/2007GL032911.

Fuller-Rowell, T., F. Wu, R. Akmaev, T.-W. Fang, and E. Araujo-Pradere (2010), A whole atmosphere model simulation of the impact of a sudden stratospheric warming on thermosphere dynamics and electrodynamics, *J. Geophys. Res.*, *115*, A00G08, doi:10.1029/2010JA015524.

Fuller-Rowell, T., R. Akmaev, F. Wu, M. Fedrizzi, R. A. Viereck, and H. Wang (2011a), Did the January 2009 sudden stratospheric warming cool or warm the thermosphere? *Geophys. Res. Lett.*, *38*, L18104, doi:10.1029/2011GL048985.

Fuller-Rowell, T., H. Wang, R. Akmaev, F. Wu, T. Fang, M. Iredell, and A. Richmond (2011b), Forecasting the dynamic and electrodynamic response to the January 2009 sudden stratospheric warming, *Geophys. Res. Lett.*, *38*, L13102, doi:10.1029/2011GL047732.

Funke, B., M. Lopez-Puertas, D. Bermejo-Pantaleon, M. Garca-Comas, G. P. Stiller, T. von Clarmann, M. Kiefer, and A. Linden (2010), Evidence for dynamical coupling from the lower atmosphere to the thermosphere during a major stratospheric warming, *Geophys. Res. Lett.*, *37*, L13803, doi:10.1029/2010GL043619.

Garcia, R. R., and S. Solomon (1985), The effect of breaking gravity waves on the dynamics and chemical composition of the mesosphere and lower thermosphere, *J. Geophys. Res.*, *90*, 3850–3868.

Goncharenko, L., and S.-R. Zhang (2008), Ionospheric signatures of sudden stratospheric warming: Ion temperature at middle latitude, *Geophys. Res. Lett.*, *35*, L21103, doi:10.1029/2008GL035684.

Goncharenko, L. P., J. L. Chau, H.-L. Liu, and A. J. Coster (2010a), Unexpected connections between the stratosphere and ionosphere, *Geophys. Res. Lett.*, *37*, L10101, doi:10.1029/2010GL043125.

Goncharenko, L. P., A. J. Coster, J. L. Chau, and C. E. Valladares (2010b), Impact of sudden stratospheric warmings on equatorial ionization anomaly, *J. Geophys. Res.*, *115*, A00G07, doi:10.1029/2010JA015400.

Goncharenko, L. P., A. J. Coster, R. A. Plumb, and D. I. V. Domeisen (2012), The potential role of stratospheric ozone in the stratosphere-ionosphere coupling during stratospheric warmings, *Geophys. Res. Lett.*, *39*, L08101, doi:10.1029/2012GL051261.

Hines, C. O. (1997a), Doppler-spread parameterization of gravity wave momentum deposition in the middle atmosphere Part 1: Basic formulation, *J. Atmos. Sol. Terr. Phys.*, *59*, 371–386.

Hines, C. O. (1997b), Doppler-spread parameterization of gravity wave momentum deposition in the middle atmosphere. Part 2: Broad and quasi monochromatic spectra, and implementation, *J. Atmos. Sol. Terr. Phys.*, *59*, 387–400.

Hong, S. S., and R. S. Lindzen (1976), Solar Semidiurnal tide in the thermosphere, *J. Atmos. Sci.*, *33*, 135–153.

Jin, H., Y. Miyoshi, D. Pancheva, P. Mukhtarov, H. Fujiwara, and H. Shinagawa (2012), Response of migrating tides to the stratospheric sudden warming in 2009 and their effects on the ionosphere studied by a whole atmosphere-ionosphere model GAIA with COSMIC and TIMED/SABER observations, *J. Geophys. Res.*, *117*, A10323, doi:10.1029/2012JA017650.

Karlsson, B., C. McLandress, and T. G. Shepherd (2009), Inter-hemispheric mesospheric coupling in a comprehensive middle atmosphere model, *J. Atmos. Sol. Terr. Phys.*, *71*, 518–530.

Limpasuvan, V., D. W. Thompson, and D. L. Hartmann (2004), The life cycle of the Northern Hemisphere sudden stratospheric warmings, *J. Clim.*, *17*, 2584–2596.

Lin, C. H., J. T. Lin, L. C. Chang, W. H. Chen, C. H. Chen, and J. Y. Liu (2013), Stratospheric sudden warming effects on the ionospheric migrating tides during 2008-2010 observed by FORMOSAT-3/COSMIC, *J. Atmos. Sol. Terr. Phys.*, *103*, 66–75, doi:10.1016/j.jastp.2013.03.026.

Lin, J. T., C. H. Lin, L. C. Chang, H. H. Huang, J. Y. Liu, A. B. Chen, C. H. Chen, and C. H. Liu (2012), Observational evidence of ionospheric migrating tide modification during the 2009 stratospheric sudden warming, *Geophys. Res. Lett.*, *39*, L02101, doi:10.1029/2011GL050248.

Lindzen, R. S. (1981), Turbulence and stress owing to gravity wave and tidal breakdown, *J. Geophys. Res.*, *86*, 9707–9714, doi:10.1029/JC086iC10p09707.

Liu, H., E. Doornbos, M. Yamamoto, and S. T. Ram (2011), Strong thermospheric cooling during the 2009 major stratosphere warming, *Geophys. Res. Lett.*, *38*, L12102, doi:10.1029/2011GL047898.

Liu, H., H. Jin, Y. Miyoshi, H. Fujiwara, and H. Shinagawa (2013), Upper atmosphere response to stratosphere sudden warming: Local time and height dependence simulated by GAIA model, *Geophys. Res. Lett.*, *40*, 635–640, doi:10.1002/grl.50146.

Liu, H.-L., and R. G. Roble (2002), A study of a self-generated stratospheric sudden warming and its mesospheric-lower thermospheric impacts using the coupled TIME-GCM/CCM3, *J. Geophys. Res.*, *107*(D23), 4695, doi:10.1029/2001JD001533.

Liu, H.-L., D. R. Marsh, C.-Y. She, Q. Wu, and J. Xu (2009), Momentum balance and gravity wave forcing in the mesosphere and lower thermosphere, *Geophys. Res. Lett.*, *36*, L07805, doi:10.1029/2009GL037252.

Liu, H.-L., W. Wang, A. D. Richmond, and R. G. Roble (2010a), Ionospheric variability due to planetary waves and tides for solar minimum conditions, *J. Geophys. Res.*, *115*, A00G01, doi:10.1029/2009JA015188.

Liu, H.-L., et al. (2010b), Thermosphere extension of the whole atmosphere community climate model, *J. Geophys. Res.*, *115*, A12302, doi:10.1029/2010JA015586.

Liu, H.-L., and A. D. Richmond (2013), Attribution of ionospheric vertical plasma drift perturbations to large-scale waves and the dependence on solar activity, *J. Geophys. Res. Space Physics*, *118*, 2452–2465, doi:10.1002/jgra.50265.

Lott, F., and M. J. Miller (1997), A new subgrid-scale orographic drag parameterization: Its formulation and testing, *Q. J. R. Meteorol. Soc.*, *123*, 101–127.

Manney, G. L., M. J. Schwartz, K. KrŸger, M. L. Santee, S. Pawson, J. N. Lee, W. H. Daffer, R. A. Fuller, and N. J. Livesey (2009), Aura Microwave Limb Sounder observations of dynamics and transport during the record-breaking 2009 Arctic stratospheric major warming, *Geophys. Res. Lett.*, *36*, L12815, doi:10.1029/2009GL038586.

Matsuno, T. (1971), A dynamical model of the stratospheric sudden warming, *J. Atmos. Sci.*, *28*, 1479–1494.

Matthias, V., P. Hoffmann, M. Rapp, and G. Baumgarten (2012), Composite analysis of the temporal development of waves in the polar MLT region during stratospheric warmings, *J. Atmos. Sol. Terr. Phys.*, *90-91*, 86–96, doi:10.1016/jastp.2012.04.004.

McFarlane, N. A. (1987), The effect of orographically excited gravity wave drag on the general circulation of the lower stratosphere and troposphere, *J. Atmos. Sci.*, *44*, 1775–1800.

McLandress, C., G. G. Shepherd, B. H. Solheim, M. D. Burrage, P. B. Hays, and W. R. Skinner (1996), Combined mesosphere/thermosphere winds using WINDII and HRDI data from the Upper Atmosphere Research Satellite, *J. Geophys. Res.*, *101*(D6), 10,441–10,453, doi:10.1029/95JD01706.

McLandress, C., J. F. Scinocca, T. G. Shepherd, M. C. Reader, and G. L. Manney (2013), Dynamical control of the mesosphere by orographic and nonorographic gravity wave drag during the extended Northern Winters of 2006 and 2009, *J. Atmos. Sci.*, *70*, 2152–2169, doi:10.1175/JAS-D-12-0297.1.

Miller, A., H. Schmidt, and F. Bunzel (2013), Vertical coupling of the middle atmosphere during stratospheric warming events, *J. Atmos. Sol. Terr. Phys.*, *97*, 11–21, doi:10.1016/j.jastp.21013.02.008.

Pedatella, N. M., and J. M. Forbes (2010), Evidence for stratosphere sudden warming-ionosphere coupling due to vertically propagating tides, *Geophys. Res. Lett.*, *37*, L11104, doi:10.1029/2010GL043560.

Pedatella, N. M., and H.-L. Liu (2013), The influence of atmospheric tide and planetary wave variability during sudden stratosphere warmings on the low latitude ionosphere, *J. Geophys. Res. Space Physics*, *118*, 5333–5347, doi:10.1002/jgra.50492.

Pedatella, N. M., H.-L. Liu, A. D. Richmond, A. Maute, and T-W. Fang (2012), Simulations of solar and lunar tidal variability in the mesosphere and lower thermosphere during sudden stratosphere warmings and their influence on the low-latitude ionosphere, *J. Geophys. Res.*, *117*(A08326), doi:10.1029/2012JA017858.

Quiroz, R. S. (1969), The warming of the upper stratosphere in February 1966 and the associated structure of the mesosphere, *Mon. Weather Rev.*, *97*, 541–552.

Sassi, F., H.-L. Liu, J. Ma, and R. R. Garcia (2013), The lower thermosphere during the Northern hemisphere winter of 2009: A modeling study using high-altitude data assimilation products in WACCM-X, *J. Geophys. Res. Atmos.*, *118*, 8954–8968, doi:10.1002/jgrd.50632.

Scherhag, R. (1952), Die explosionsartige Stratosphärenerwarmung des Spätwinters 1951/52, *Ber. Deut. Wetterdieustes*, *6*, 51–63.

Schmidt, H., G. P. Brasseur, M. Charron, E. Manzini, M. A. Giorgetta, T. Diehl, V. I. Fomichev, D. Kinnison, D. Marsh, and S. Walters (2006), The HAMMONIA chemistry climate model: Sensitivity of the mesopause Region to the 11-year solar cycle and CO_2 doubling, *J. Clim.*, *19*, 3903–3931.

Schoeberl, M. R. (1978), Stratospheric warmings: Observations and theory, *Rev. Geophys.*, *16*(4), 521–538, doi:10.1029/RG016i004p00521.

Schunk, R. W., L. Gardner, L. Scherliess, and L. Zhu (2012), Problems associated with uncertain parameters and missing physics for long-term ionosphere-thermosphere forecasting, *Radio Sci.*, *47*, RS0L23, doi:10.1029/2011RS004911.

Schwartz, M. J., et al. (2008), Validation of the aura microwave limb sounder temperature and geopotential height measurements, *J. Geophys. Res.*, *113*, D15S11, doi:10.1029/2007JD008783.

Smith, A. K. (2003), The origin of stationary planetary waves in the upper mesosphere, *J. Atmos. Sci.*, *60*, 3033–3041.

Sridharan, S., S. Sathishkumar, and S. Gurubaran (2012), Variabilities of mesospheric tides during sudden stratospheric warming events of 2006 and 2009 and their relationship with ozone and water vapour, *J. Atmos. Sol. Terr. Phys.*, *78*, 108–115, doi:10.1016/j.jastp.2011.03.013.

Tan, B., X. Chu, H.-L. Liu, C. Yamashita, and J. M. Russell III (2012), Zonal-mean global teleconnection from 15 to 110 km derived from SABER and WACCM, *J. Geophys. Res.*, *117*, D10106, doi:10.1029/2011JD016750.

Wang, H., T. J. Fuller-Rowell, R. A. Akmaev, M. Hu, D. T. Kleist, and M. D. Iredell (2011), First simulations with a whole atmosphere data assimilation and forecast system: The january 2009 major sudden stratospheric warming, *J. Geophys. Res.*, *116*, A12321, doi:10.1029/2011JA017081.

Zülicke, C., and E. Becker (2013), The structure of the mesosphere during sudden stratospheric warmings in a global circulation model, *J. Geophys. Res. Atmos.*, *118*, 2255–2271, doi:10.1002/jgrd.50219.